Bulgarian Chemical Communications, Volume 56, Issue 4 (pp. 369-378) 2024 *DOI: 10.34049/bcc.56.4.5603*

Thin film humidity sensing elements based on TiO_2 and graphene

Z. P. Nenova[1*], S. V. Kozhukharov[2], T. G. Nenov[1], N. D. Nedev[1]

[1] *Technical University of Gabrovo, 4, Hadzhi Dimitar Str., 5300, Gabrovo, Bulgaria*
[2] *University of Chemical Technology and Metallurgy, 8, St. Kliment Ohridski Blvd., 1756, Sofia, Bulgaria*

Received: September 02, 2023; Revised: July 05, 2024

Thin film humidity sensing elements based on TiO_2 and graphene prepared *via* a sol-gel method were developed. Titanium (IV) n-butoxide (TBOT) and graphene nanoplatelet aggregates (GNPs) were used as basic materials. The samples were sintered at 400°C, 600°C and 800°C. The map data analyses of the surface layer materials were carried out by energy dispersive X-ray (EDX) spectroscopy and the structural characterization – by X-ray diffractometry (XRD). The electrical properties of the sintered sensing elements were investigated in the range of 17% to 85% relative humidity at 20 Hz and 25°C. The experimental results were analyzed for groups of samples with different initial graphene content depending on the sintering temperature (400°C, 600°C and 800°C). The obtained characteristics show that at all investigated sintering temperatures the proposed samples based on TiO_2 and graphene surface layers have a wider range of variation of their resistance R to humidity, as well as a lower resistance compared to the corresponding reference samples without graphene. The maximum relative sensitivity $S_{Rrel\ max}$ is highest for the samples sintered at 400°C and 600°C with a higher amount of graphene in the preparation and reaches up to about 735 and 501, respectively, and the resistance variation range - up to about 3 orders of magnitude.

Keywords: humidity sensing elements, sol-gel method, titanium dioxide, graphene

INTRODUCTION

Humidity measurement and control are widely used in industry and agriculture, storage of various products, meteorology, medicine and health care, environmental protection, etc. [1, 2]. Sensors are an important part of humidity measuring devices, with a constant aim at improving their parameters and characteristics.

Resistive sensors are widely used among humidity sensors, most often based on oxide materials such as Al_2O_3 [3, 4], TiO_2 [5-8], SnO_2 [9-12], ZnO [13-15], SiO_2 [16-18], etc. TiO_2 is one of the oxides used for development of the sensitive elements of humidity sensors due to its good hydrophilicity. To improve the characteristics of the sensor elements, various alloying additives are used [19].

Since its discovery in 2004 [20], graphene has been explored for various applications due to its unique electrical, thermal, and mechanical properties. Research has also been conducted on its application in sensors [21, 22]. The study in [23] examines the humidity sensitivity of graphene/TiO_2 composites prepared by sol-gel technology and sintered at 400°C. A humidity sensor based on graphene oxide films supported by TiO_2 nanorods has been investigated in [24].

In the present work, thin film humidity sensing elements based on TiO_2 and graphene prepared by a sol-gel method are proposed. Their preparation follows an uncomplicated procedure and affordable materials, namely titanium (IV) n-butoxide (TBOT) as a precursor of TiO_2 and graphene aggregates of nanoplatelets (GNPs) as an additive. The influence of the amount of graphene additive and of the sintering temperature (400°C, 600°C and 800°C) on the electrical resistance and humidity sensitivity of the sensor elements is investigated in order to obtain groups of sensitive elements with improved humidity sensing properties.

EXPERIMENTAL

Sample preparation

The preparation of the studied sensing elements is divided into three subsequent stages: (i) sol systems preparation; (ii) film deposition and gelation and (iii) final sample sintering.

(i) Sol systems preparation

The following materials were used for the sol-gel systems preparation: titanium (IV) n-butoxide (TBOT), produced by Alfa Aesar, graphene nanoplatelet aggregates (GNPs) produced by Alfa Aesar, 1-butanol 99% and nitric acid 65%.

* To whom all correspondence should be sent:
E-mail: z_nenova@yahoo.com

Initially, mixtures of 30 ml of butanol, 30 ml of TBOT and 3 ml of nitric acid were prepared in two separate beakers by intensive shaking. To one of the mixtures 6.0599 g of graphene (GNPs) was added. In this way, two solutions were prepared, without and with graphene addition, which are denoted as reference solution and base solution with graphene, respectively. Both vessels were placed in an ultrasonic bath for 1 hour.

After that, different amounts of the obtained solutions were poured into 3 test tubes and the following compositions were obtained: TiR - 20 ml reference solution; TiG1 - 10 ml reference solution and 10 ml base solution with graphene; TiG2 - 20 ml base solution with graphene. The resulting compositions were left for 2 hours at 75°C.

(ii) Film deposition and gelation

Prior to the deposition process, the respective solutions were heated for 30 min at 75°C. The deposition was carried out on alumina substrates with symmetrical interdigital silver-palladium electrodes with an electrode width and distance between them of 0.5 mm [8], pre-cleaned by immersion in ether overnight. The layers were deposited by sixfold dipping in test tubes. This procedure was performed by subsequent exposure of the specimens to the solutions for 15 min, and 15 min drying at 75°C. The last drying was performed for 30 min. Finally, the samples were left to ambient conditions at least overnight, in order to achieve the final gelation of the films.

(iii) Final sample sintering

After gel deposition, the samples were sintered at 400°C, 600°C and 800°C for 30 min.

Additionally, after deposition on the ceramic substrates, the gels were placed in Petri dishes and, to convert them into powders, they were sintered for subsequent XRD analysis at the same temperatures as the samples.

In the designations of samples and powder materials, the sintering temperature is added as "_xxx" to the entered abbreviation of the corresponding group of samples with a given composition: TiR_xxx, TiG1_xxx and TiG2_xxx.

Surface morphology and structural characterization

Morphological observations of the surface layers of the developed samples were taken by scanning electron microscopy (SEM) combined with elemental analysis, by TESCAN, SEM/FIB LYRA I XMU working at 20 kV at magnification ×5000. The map data analyses were carried out by energy dispersive spectroscopy (EDX) using an energy dispersive spectrometer (Quantax 200 of Bruker detector).

Structural and compositional characterization was performed by X-ray diffraction analysis (XRD) on powder materials from the respective gels for the separate groups of samples, TiR, TiG1 and TiG2, sintered at 400°C, 600°C and 800°C. The studies were carried out on a Philips PW 1050 instrument equipped with a CuKα-X-ray emitter and a monochromator of diffracted radiation within the angle range (2θ) from 7° to 95° with a step of 0.05°2θ.

Electrical measurements

The measurements of the electrical resistance *R* of the developed samples were taken on a precision impedance analyzer 6505P of Wayne Kerr Electronics Ltd., at a frequency of the excitation signal of 20 Hz and 500 mV at 25°C. The samples were put inside a humidity/temperature conditioning chamber VAPORTRON H-100BL manufactured by Buck Research Instruments L.L.C., which provides conditioning of accurately controlled humidity in the range of 15–93% with maximal deviation of up to ±1.5% of relative humidity at a given temperature.

RESULTS AND DISCUSSION

SEM and EDX analyses

The obtained SEM and EDX images during the observations of the surface layers of the investigated samples TiR, TiG1 and TiG2 sintered at temperatures 400°C, 600°C and 800°C are presented in Fig. 1.

The SEM-images show that surface layers consisting of the individual aggregates of the sintered material separated by channel-like spaces are observed in all samples. These channel-shaped spaces grow at a sintering temperature of 800°C for the samples with the presence of graphene in the starting material. They contribute to the occurrence of capillary condensation, and as the size increases, the relative humidity levels at which these processes begin, increase.

The EDX images confirm the presence of Ti and O in the surface layers of all sample types, with C also present for samples TiG1 and TiG2.

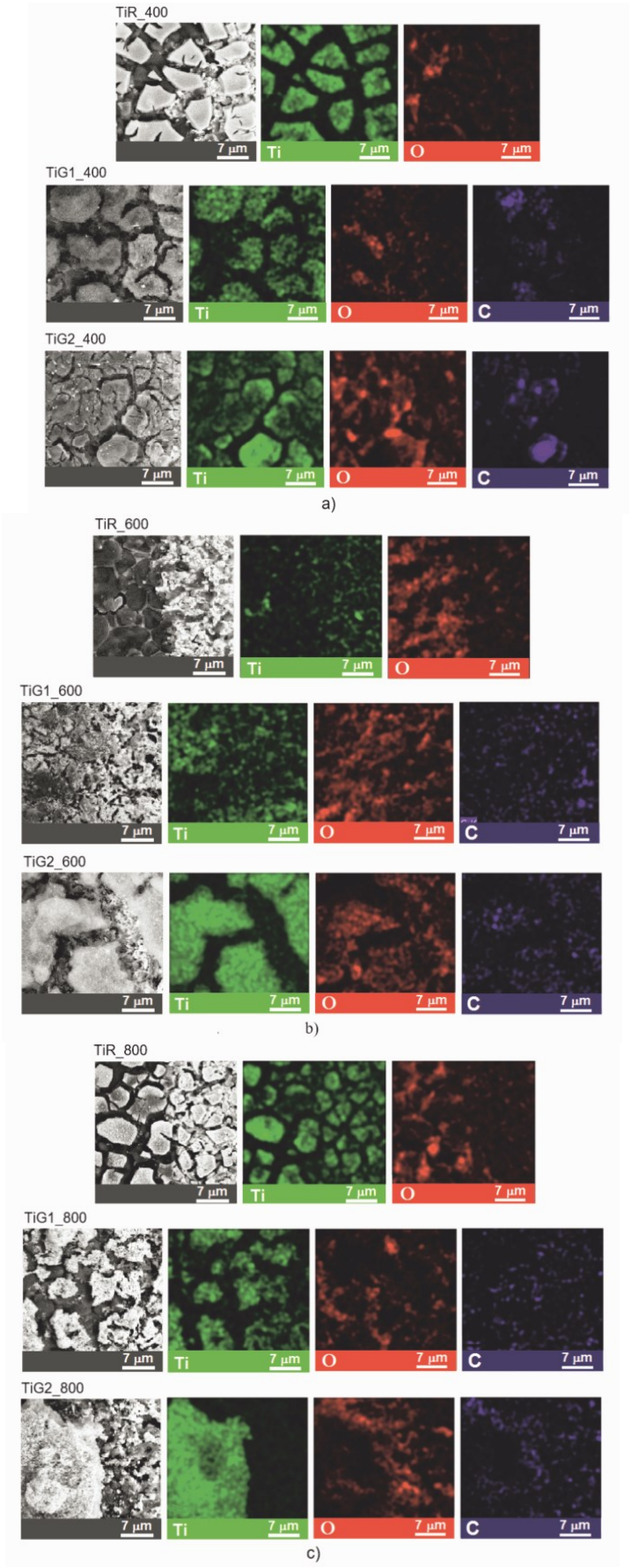

Fig. 1. SEM and EDX images of the surface layers of samples TiR, TiG1 and TiG2 sintered at temperatures of: a) 400°C, b) 600°C and c) 800°C

XRD analysis

The XRD patterns of the materials of the investigated samples TiR, TiG1 and TiG2 for each of the sintering temperatures are presented in Fig. 2.

At a sintering temperature of 400°C for all TiR, TiG1 and TiG2 samples, regardless of the absence or presence of graphene in the preparation, the material structure of the surface layers corresponds to TiO_2 – anatase (PDF code: 01-071-1169). At 600°C, a transformation to rutile begins for all samples and the structure includes TiO_2 - anatase and rutile (PDF code: 01-078-1510). At 800°C, for TiR samples without the presence of graphene in the preparation, the structure of the samples contains rutile, and for TiG1 and TiG2 it includes TiO_2 – rutile and smaller amounts of anatase. For samples TiG1 and TiG2, sintered at 400°C, 600°C and 800°C, XRD studies also show the presence of graphite (PDF code: 00-026-1079). As noted in [25], at temperatures between 550°C and about 1000°C, anatase is irreversibly converted into the equilibrium rutile phase and the temperature of this transformation depends on the impurities or dopants present. In the case under consideration, in the material of the reference samples, the transformation to rutile was completed at 800°C, while in the presence of graphene additive in the preparation of the samples, the materials sintered at 800°C, along with rutile, still contained anatase.

Since there is a difference in the profiles of the diffraction lines, the crystallite sizes of anatase and rutile were calculated according to the Scherrer equation [26] from the measured half-width of the lines. For samples TiR, TiG1, TiG2 sintered at 400°C, the sizes of anatase crystallites are 6 nm, 6 nm, 5 nm, respectively; at 600°C - of anatase crystallites: 22 nm, 21 nm, 21 nm; at 800°C – for the samples with graphene, of anatase crystallites: 27 nm, 27 nm, of rutile crystallites for the three types of samples: 35 nm, 33 nm, 32 nm. There is no significant difference between the crystallite sizes of anatase and rutile for the respective groups at the same sintering temperatures.

Crystallite sizes increase with increasing sintering temperature. This increase may also result in an increase in the intercrystallite spaces, which would affect the sensitivity at different relative humidity levels.

Electrical characteristics

The characteristic $R = f(RH)$ of the resistance R *versus* the relative humidity RH for the individual groups of samples TiR, TiG1 and TiG2 at sintering temperatures of 400°C, 600°C and 800°C, investigated at 20 Hz and 25ºC in the range of (17-85)% RH, are presented in Fig. 3. They allow to follow the influence of the initial amounts of graphene in the preparation of the samples on the corresponding characteristics.

The maximum relative variation (R_{max}/R_{min}) of the parameter R of the humidity sensing elements in the range from RH_{min} to RH_{max} can be assumed to be the maximum relative sensitivity:

$$S_{Rrel\ max} = R_{max}/R_{min} \quad (1)$$

over the entire RH range with respect to resistance.

The range of resistance variation in orders of magnitude can be calculated as:

$$L_R = lg\ (R_{max}/R_{min}) = lg\ (R_{max}) - lg\ (R_{min}) \quad (2)$$

For the studied samples, in the range of (17-85)% RH the maximum relative sensitivity $S_{Rrel\ max}$ and the resistance variation range L_R in orders of magnitude are presented in Table 1.

Table 1. Maximum relative sensitivity $S_{Rrel\ max}$ and resistance variation range L_R

Sample	$S_{Rrel\ max}$, -	Resistance variation range L_R, orders of magnitude
TiR_400	22.4	1.35
TiG1_400	406.20	2.61
TiG2_400	735.84	2.87
TiR _600	5.65	0.75
TiG1_600	155.65	2.19
TiG2_600	501.73	2.70
TiR _800	2.56	0.41
TiG1_800	73.43	1.86
TiG2_800	105.27	2.02

For samples TiG1 and TiG2 prepared with the addition of graphene, at all sintering temperatures their maximum relative sensitivity $S_{Rrel\ max}$ increased compared to that of the reference samples TiR, this increase being about 33 times at 400° C, 88 times at 600° C and 41 times at 800° C. For the reference samples, the relative change in R was about 1.4 orders of magnitude at 400°C, about 0.8 orders of magnitude at 600°C, and about 0.4 orders of magnitude at 800°C. This variation for TiG1 samples was about 2.6 orders of magnitude at 400°C, about 2 orders of magnitude at 600°C and 800°C, while for TiG2 samples it reached about 3 orders of magnitude at 400°C and 600°C and about 2 orders of magnitude at 800°C sintering temperatures.

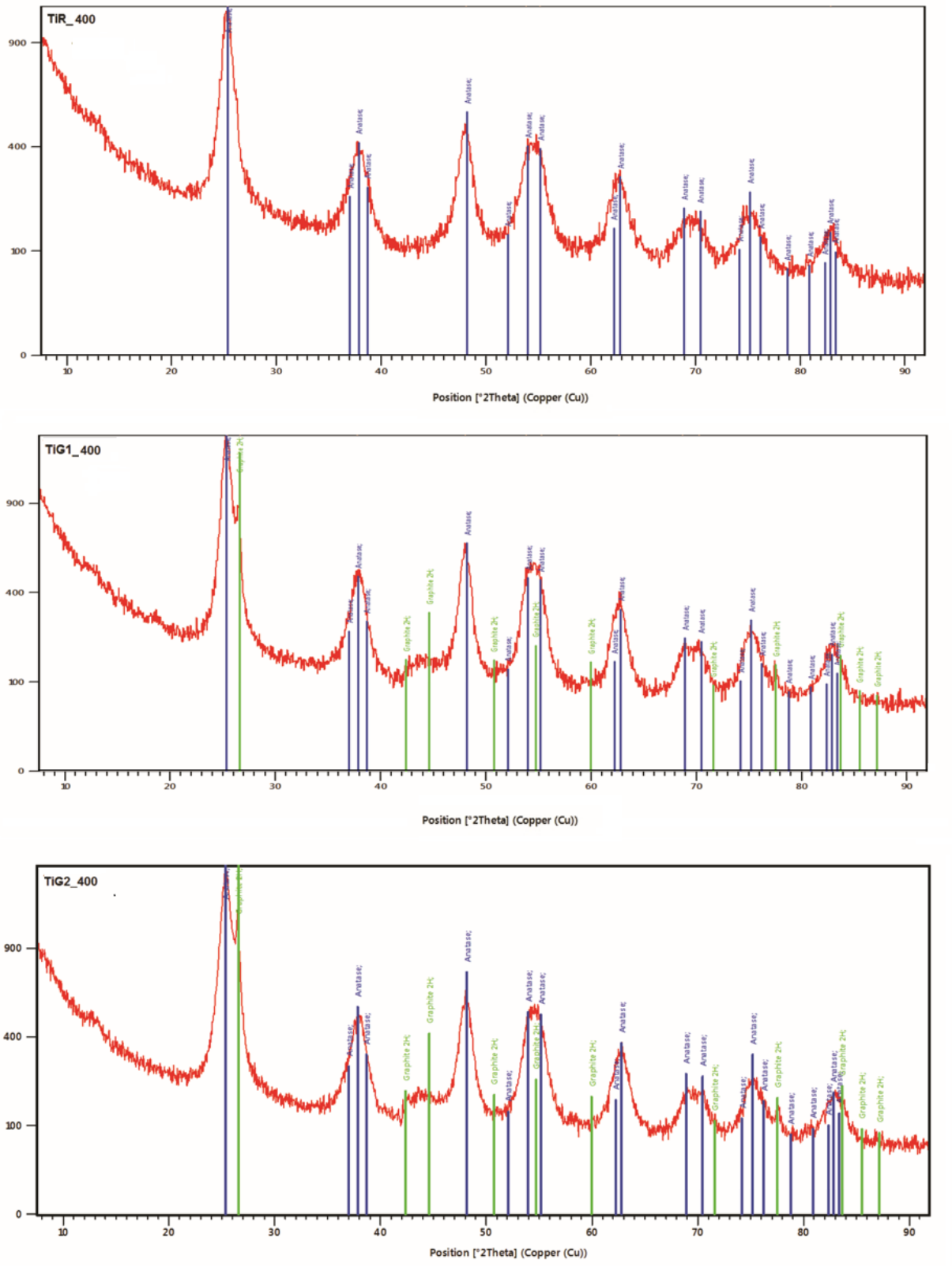
TiR_400
TiG1_400
TiG2_400
Position [°2Theta] (Copper (Cu))
Anatase;
Graphite 2H;

a)

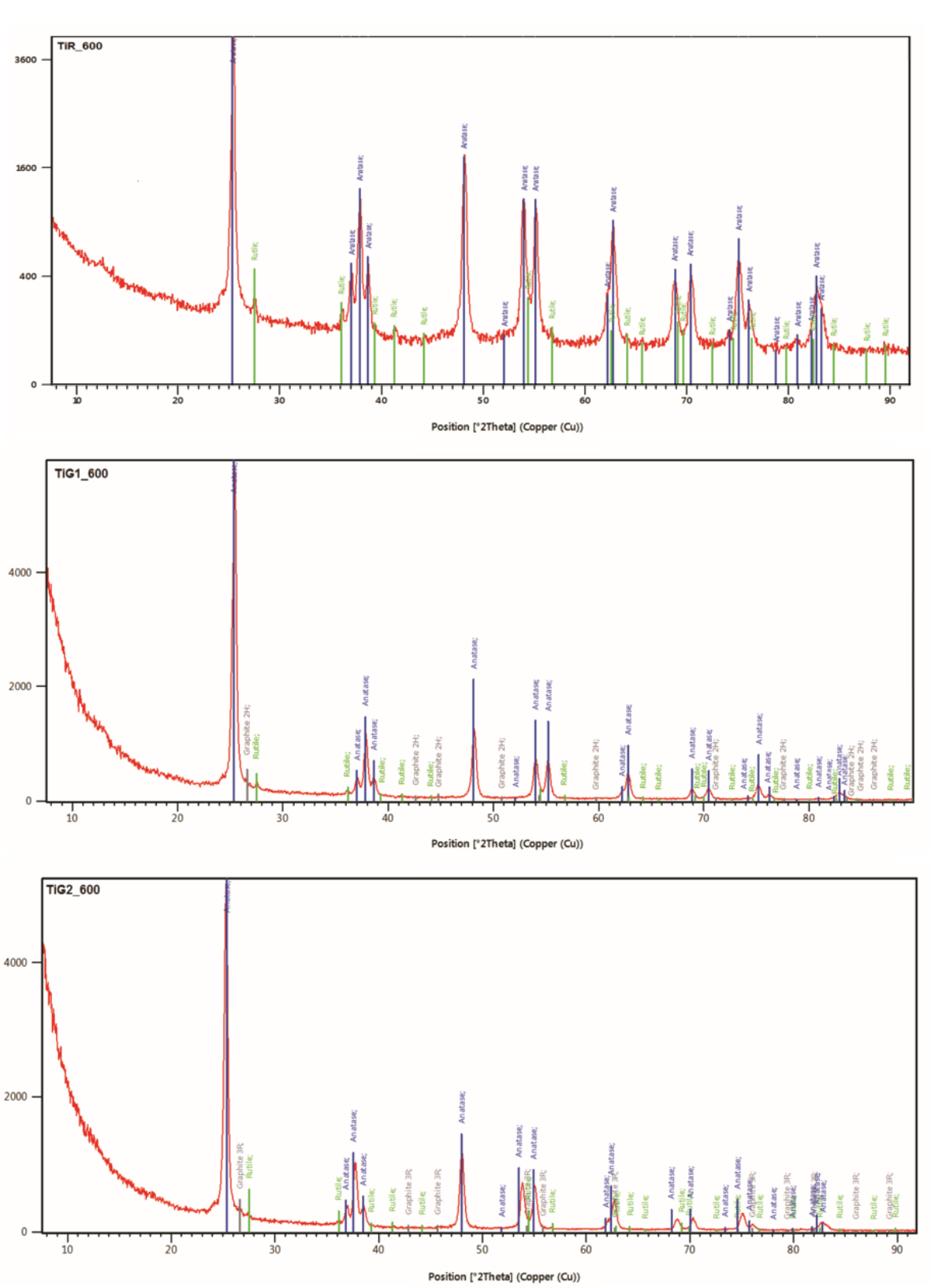
TiR_600
Position [°2Theta] (Copper (Cu))
TiG1_600
Position [°2Theta] (Copper (Cu))
TiG2_600
Position [°2Theta] (Copper (Cu))

b)

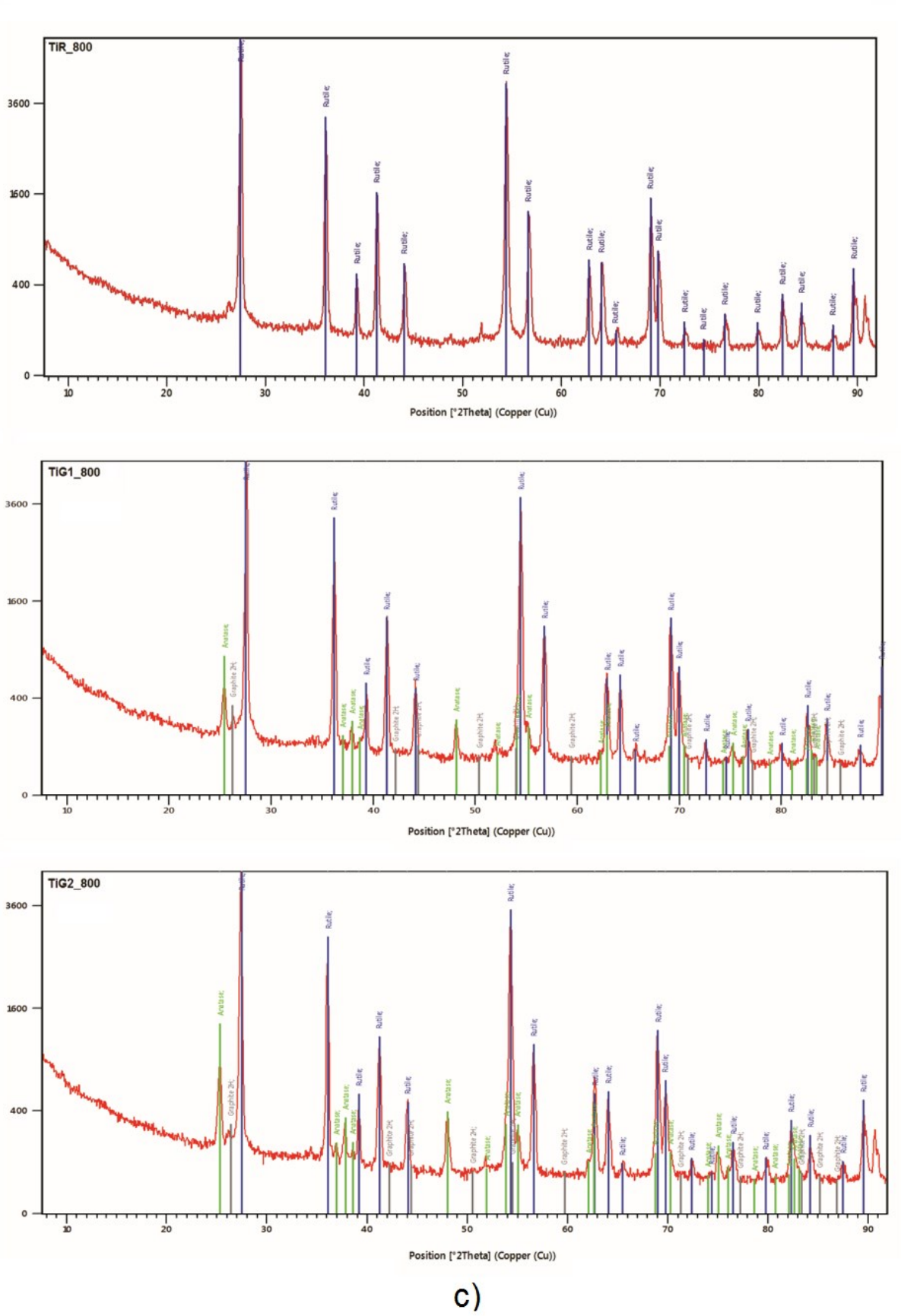

Fig. 2. XRD images of the materials of samples TiR, TiG1 and TiG2 sintered at temperatures of: a) 400°C, b) 600°C and c) 800°C

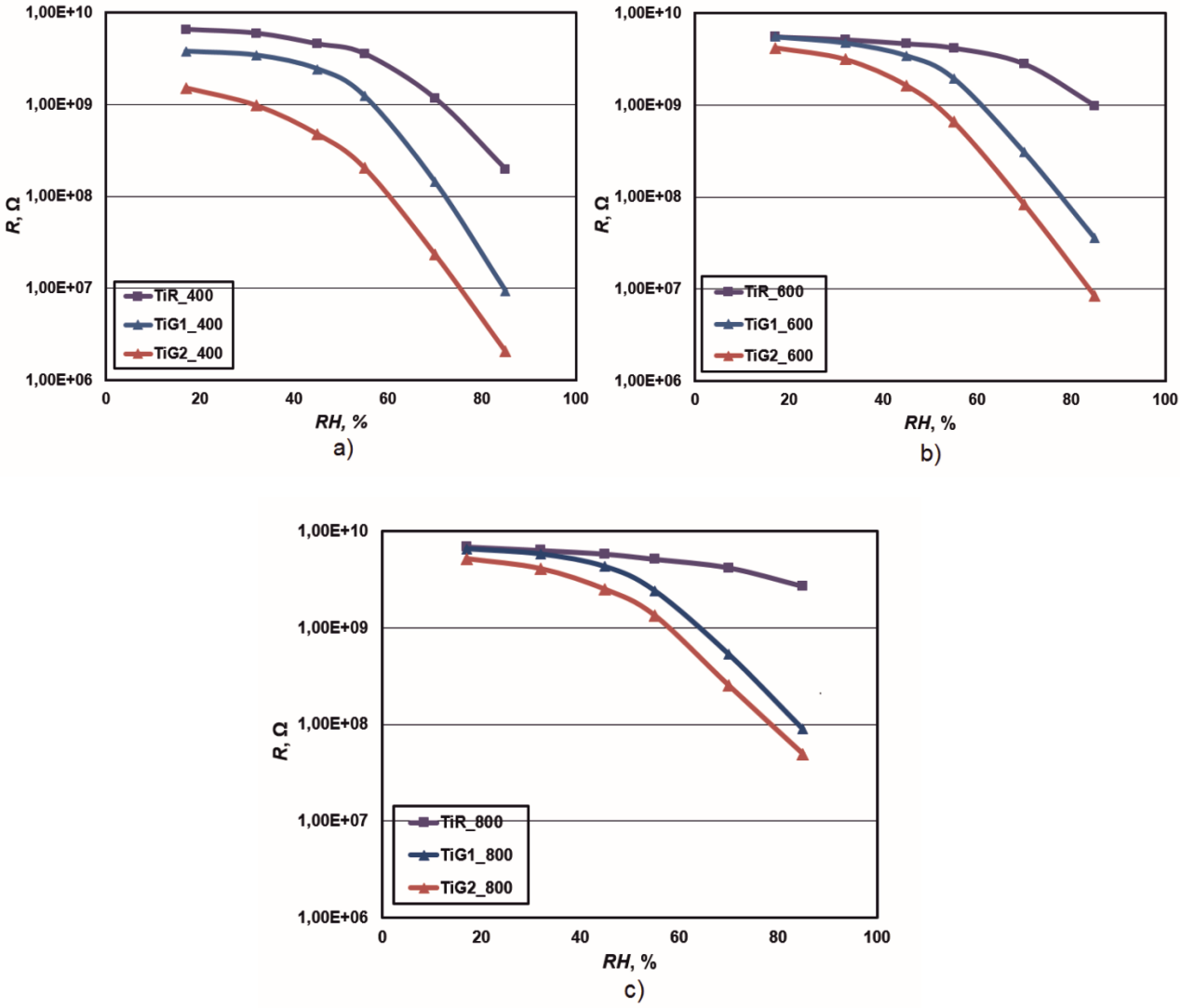

Fig. 3. Characteristic $R = f(RH)$ for samples TiR, TiG1 and TiG2 at sintering temperatures of: a) 400°C; b) 600°C and c) 800°C, investigated at 20 Hz and 25ºC.

Moreover, the increase in the graphene content during the preparation of the sensitive layers leads to a certain decrease in their resistance due to the appearance of graphite in the aggregates in the surface layers after sintering the samples. This is favorable for the connection of the sensing elements in measurement circuits.

For all investigated sintering temperatures of 400°C, 600°C and 800°C, the samples in the presence of graphene additive have improved properties compared to the reference samples. At a given sintering temperature, a greater variation of the resistance and a higher sensitivity of the samples started to appear at lower relative humidity levels with increasing initial amounts of graphene, where the steepness of the characteristics (Fig. 3) on a semi-logarithmic scale becomes more significant.

At higher sintering temperatures and a set initial amount of graphene in the preparation of the samples, a relatively higher resistance was observed, associated with an increase in the spaces between the aggregates in the surface layers, best expressed at 800°C.

Regarding the $S_{Rrel\ max}$ of the samples, at 800°C sintering temperature, a certain decrease in this variation was observed for each of the sample groups with the same initial amount of graphene due to an increase in the intercrystalline spaces and in the spaces between the surface aggregates, therefore the processes of capillary condensation of water vapor in accordance with Kelvin's equation [27] and sensitivity begin to manifest themselves at higher relative humidity levels. Furthermore, increasing the sintering temperature leads to a transformation of the TiO_2 structure from anatase to rutile, as noted in the XRD-analysis results. The use of initial amounts of graphene additives leads to the fact that at 800°C there is still the presence of anatase in the structure

of the obtained layers, as noted above [25]. In accordance with [28], the anatase structure of TiO_2 favors its hygroscopic properties.

Due to these factors, a larger relative change of the resistance *R* with the change of relative humidity RH is observed at sintering temperatures of 400°C and 600°C, and this is best expressed in TiG2 samples with larger initial amounts of graphene (TiG2_400 and TiG2_600), the resistance variation range reaching about 3 orders of magnitude when relative humidity changes from 17% RH to 85% RH.

CONCLUSIONS

It was established that for the developed samples based on TiO_2 and graphene, prepared by a sol-gel method, the increase in the initial amounts of graphene leads to an increase in the maximum relative resistance variation, respectively – maximum relative sensitivity $S_{Rrel\,max}$ of the samples and to a decrease of their resistance. For all investigated sintering temperatures, for the groups of sensor elements with the presence of graphene in the starting solution, an increase in the maximum relative resistance variation with respect to humidity was observed compared to the reference samples without the presence of graphene additive.

The highest maximum relative sensitivity $S_{Rrel\,max}$ to humidity is observed in the samples with larger initial amounts of graphene at 400°C and 600°C sintering temperatures (TiG2_400 and TiG2_600) – about 735 and 501, respectively, and the relative resistance variation range L_R reaches about 3 orders of magnitude (2.9 and 2.7 orders of magnitude, respectively). With smaller amounts of graphene, a relative resistance change of about 2.6 orders of magnitude is observed at a lower sintering temperature – 400°C (TiG1_400) and about 2.2 orders of magnitude - at 600°C (TiG1_600). For the remaining samples from the two groups at sintering temperature 800°C (TiG1_800 and TiG2_800), the relative resistance change is in the range of about 2 orders of magnitude (1.9 and 2.0 orders of magnitude, respectively).

The developed sensor elements have good humidity properties, are made of inexpensive materials by a simple technology, which makes them suitable for practical applications.

Acknowledgement: *The present study was made possible thanks to the support by the European Regional Development Fund under the OP "Science and Education for Smart Growth 2014 - 2020," Project CoC "Smart Mechatronic, Eco- and Energy Saving Systems and Technologies" Grant number BG05M2OP001-1.002-0023.*

REFERENCES

1. R. Wernecke, J. Wernecke, Industrial Moisture and Humidity Measurement: A Practical Guide, Wiley-VCH Verlag GmbH & Co, Weinheim, 2014.
2. P. Wiederhold, Water Vapour Measurement: Methods and Instrumentation, Marcel Dekker, New York, 1997.
3. G. Sberveglieri, R. Anchisini, R. Murri, C. Ercoli, N. Pinto, *Sens. Actuators B Chem.*, **32**, 1 (1996).
4. B. Cheng, B. Tian, C. Xie, Y. Xiao, S. Lei, *J. Mater. Chem.*, **21**, 1907 (2011).
5. T. Nenov, Z. Nenova, *Ceram. Int.*, **39**, 4465 (2013).
6. Y. Hase, V. Sharma, V. Doiphode et al., *J. Mater. Sci.: Mater. Electron.*, **33**, 11825 (2022).
7. M. M. Zahidi, M. H. Mamat, M. F. Malek, M. K. Yaakob, M. K. Ahmad, S. A. Bakar, A. Mohamed, A S. R. A Subki, M. R. Mahmood, *Sens.*, **22**, 5794 (2022).
8. S. Kozhukharov, Z. Nenova, T. Nenov, N. Nedev, M. Machkova, *Sens. Actuators B Chem.*, **210**, 676 (2015).
9. S. Pan, G. Gayathri, T.S. Reshma, G. Mangamma, A. K. Prasad, A. Das, *Sens. Actuators A Phys.,* **346**, 113835 (2022).
10. D. Toloman, A. Popa, M. Stan, C. Socaci, A. R. Biris, G. Katona, F. Tudorache, I. Petrila, F. Iacomi, *Appl. Surf. Sci.*, **402**, 410 (2017).
11. M. Parthibavarman, V. Hariharan, C. Sekar, *Mater. Sci. Eng. C,* **31**, 840 (2011).
12. Q. Kuang, C. Lao, Z. L. Wang, Z. Xie, L. Zheng, *J. Am. Chem. Soc.*, **129**, 6070 (2007).
13. S. Yu, H. Zhang, C. Chen, C. Lin, *Sens. Actuators B Chem.*, **287**, 526 (2019).
14. S. P. Gupta, A. S. Pawbake, B. R. Sathe, D. J. Late, P. S. Walke, *Sens. Actuators B Chem.*, **293**, 83 (2019).
15. E. Modaresinezhad, S. Darbari, *Sens. Actuators B, Chem.*, **237**, 358 (2019).
16. H. Zhao, T. Zhang, R. Qi, J. Dai, S. Liu, T. Fei, G. Lu, *Sens. Actuators B Chem.*, **266**, 131 (2018).
17. Z. Nenova, T. Nenov, S. Kozhukharov, N. Nedev. *IEEE Sensors J.*, **18** (17), 6946 (2018).
18. Z. P. Nenova, S. V. Kozhukharov, T. G. Nenov, N. D. Nedev, M. S. Machkova. *Bulg. Chem. Commun.*, **45,** Special Edition **A,** 11 (2013).
19. A. Farzaneh, A. Mohammadzadeh, M. D. Esrafili, O. Mermer, *Ceram. Int.,* **45**, 8362 (2019).
20. K. S. Novoselov, A. K. Geim, S. V. Morozov, D. Jiang, Y. Zhang, S. V. Dubonos, I. V. Grigorieva, A. A. Firsov, *Science,* **306**, 666 (2004).
21. D. Shahdeo, A. Roberts, N., S. Gandhi, *Compr. Anal. Chem.*, **91**, 175 (2020).
22. A. Naga, A. Mitra, S. C. Mukhopadhyay, *Sens. Actuators B Chem.*, **270**, 177 (2018).
23. W.-D. Lin, C.-T. Liao, T.-C. Chang, S.-H. Chen, R.-J. Wu, *Sens. Actuators B, Chem.*, **209**, 555 (2015).
24. X. Zhao, X. Chen, X. Yu, X. Ding, X. Yu, X. Chen, *Diam. Relat. Mater.*, **109**, 108031 (2020).
25. A. H. Dorian, C. C. Sorrell, *J. Mater. Sci.,* **46**, 855 (2011).

26. P. Scherrer, *Göttinger Nachrichten Gesell.*, **2**, 98 (1918).
27. Y. Shimizu, H. Arai, T. Seiyama, *Sens. Actuators,* **7**, 11 (1985).
28. B. Fubini, V. Bolis, M. Bailes, F. S. Stone, *Solid State Ion.*, **32–33**, 258, Part 1 (1989).